THE JOURNAL OF PHYSICAL CHEMISTRY B

Article

pubs.acs.org/JPCB

Slow Aromatic Ring Flips Detected Despite Near-Degenerate NMR Frequencies of the Exchanging Nuclei

Ulrich Weininger,[†] Michal Respondek,[†] Christian Löw,[‡] and Mikael Akke*,[†]

[†]Department of Biophysical Chemistry, Center for Molecular Protein Science, Lund University, P.O. Box 124, SE-221 00 Lund, Sweden

[‡]Department of Medical Biochemistry and Biophysics, Karolinska Institute, SE-171 77 Stockholm, Sweden

Supporting Information

ABSTRACT: Aromatic ring flips of Phe and Tyr residues are a hallmark of protein dynamics with a long history in molecular biophysics. Ring flips lead to symmetric exchange of nuclei between sites with distinct magnetic environments, which can be probed by NMR spectroscopy. Current knowledge of ring-flip rates originates from rare cases in which the chemical shift difference between the two sites is sufficiently large and the ring-flip rate sufficiently slow, typically $k_{flip} < 10^3$ s^{-1}, so that separate peaks are observed in the NMR spectrum for the two nuclei, enabling direct measurement of the flip rate. By contrast, a great majority of aromatic rings show single peaks for each of the pairs of δ or ε nuclei, which commonly are taken as inferential evidence that the flip rate is fast, $k_{flip} \gg 10^3$ s^{-1}, even though rate measurements have not been achieved. Here we report a novel approach that makes it possible to identify slow ring flips in previously inaccessible cases where only single peaks are observed. We demonstrate that Y21 in the bovine pancreatic trypsin inhibitor (BPTI) has a slow ring-flip rate, $k_{flip} < 100$ s^{-1}, a result that contrasts with previous estimates of 10^4–10^6 s^{-1} inferred from the single-peak spectrum of Y21. Comparison with a recent 1 ms molecular dynamics trajectory of BPTI shows qualitative agreement and highlights the value of accurate aromatic ring flip data as an important benchmark for molecular dynamics simulations of proteins across wide time scales.

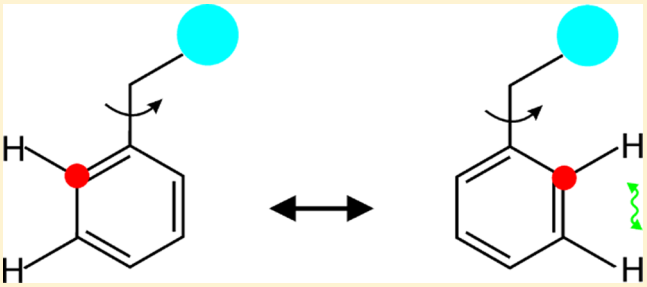

INTRODUCTION

Aromatic residues form a versatile subgroup of the 20 amino acid residues commonly found in proteins. They contribute a significant part (roughly 25% of the volume on average) of the hydrophobic core, where they are typically involved in specific aromatic–aromatic pair interactions or clusters of three or more aromatic residues, which show a clear preference for a pairwise edge-to-centroid (orthogonal) orientation.[1] Despite the dense packing of protein interiors, many Phe and Tyr residues apparently undergo frequent 180° rotations ("ring flips") of the χ_2 dihedral angle, i.e., around the C^{β}–C^{γ}–C^{ζ} axis, as documented in landmark NMR studies on protein dynamics by early pioneers in the field.[2−4] Ring flips require that the surrounding protein core undergoes concerted "breathing" motions with relatively large activation volumes.[5−7] Detailed characterization of ring flips therefore provides a rich source of information on the conformational fluctuations of proteins in terms of rate constants, energy barriers, and activation volumes,[5−10] which serve as important benchmarks for molecular dynamics (MD) trajectories across a wide range of time scales.[11,12] Thus, there is a strong motivation to extend the experimental repertoire of methods used for studying aromatic ring flips in order to both generate biophysical insight and provide accurate data for benchmarking.

Conformational exchange on the millisecond to second time scales can be characterized by NMR relaxation dispersion experiments.[13,14] Exchange contributions to the transverse relaxation rates are caused by modulation of the chemical shift[15] or residual dipolar coupling[16,17] that occurs as a consequence of conformational changes. Monitoring the transverse relaxation rate as a function of the frequency of refocusing pulses in the Carr–Purcell–Meiboom–Gill (CPMG) sequence[18,19] makes possible the determination of the exchange rate, k_{ex}, the relative populations of the exchanging states, p_i, and the difference in chemical shifts, $\Delta\omega$, or residual dipolar couplings between them.[13,14] A number of important biological problems have been addressed using CPMG experiments targeting primarily the protein backbone or methyl groups.[20−25] To introduce novel probes of conformational dynamics, we recently presented a set of longitudinal and transverse relaxation-optimized pulse sequences tailored for aromatic ^{13}C relaxation, including the longitudinal and transverse relaxation-optimized spectroscopy CPMG (L-TROSY-CPMG) experiment.[26,27]

Received: June 14, 2013
Revised: July 15, 2013
Published: July 16, 2013

   dx.doi.org/10.1021/jp4058065 | J. Phys. Chem. B 2013, 117, 9241–9247

Experimental measurements of ring-flip rates have been limited to a handful of cases that show separate peaks for each pair of δ or ε nuclei (in ring positions 2 and 6 or 3 and 5, respectively), indicating that the flip rate is slow on the chemical shift time scale, i.e., it is less than the chemical shift difference between the two sides of the ring, $k_{flip} < |\omega_1 - \omega_2|$, with published data indicating $k_{flip} \approx 10^1 - 10^2$ s^{-1}.[5−10] This scenario occurs for only a few percent of the total number of aromatic chemical shift assignments deposited in the biological magnetic resonance data bank (BMRB).[28] In contrast, the NMR spectrum of Phe and Tyr typically reveals a single peak for each pair of δ or ε nuclei, suggesting that the flip rate is fast on the chemical shift time scale, $k_{flip} > |\omega_1 - \omega_2|$. Given the distribution of chemical shift differences between nondegenerate ^{1}H pairs, where 95% of the data falls within the range 0.05−1.4 ppm,[29] as well as the total variance of about 2.6 ppm for δ or ε chemical shifts of ^{13}C or ^{1}H (including degenerate shifts) in the BMRB, one might expect that the great majority of rings showing a single peak for each pair of nuclei should have flip rates on the order of at least 10^3 s^{-1} at ambient temperature. Indeed, the observation of single δ and ε peaks is commonly taken as evidence that the ring-flip rate is fast, $k_{flip} > 10^3$ s^{-1}.[2−4] Careful analysis of resonance broadening at low temperatures has yielded probabilistic measures of the lower bounds of ring-flip rates.[29] However, direct characterization of ring-flip rates has not previously been achieved for aromatic residues showing single-peak NMR spectra. Here we introduce a novel approach based on the ^{13}C L-TROSY-CPMG experiment,[27] which uniquely enables identification of slow ring flips for aromatic residues even though the exchanging nuclei have virtually degenerate chemical shifts. Using this method, we demonstrate that the aromatic ring of Y21 in BPTI has a flip rate of less than 100 s^{-1}, which is 2−4 orders of magnitude slower than previously published rates for this residue.

MATERIALS AND METHODS

Protein Sample Preparation. The BPTI sample contained 8 mM protein with natural abundance isotope composition dissolved in water at pH 7.1. SlyD was expressed and purified as described,[30] using 1-$^{13}C_1$-glucose or 2-$^{13}C_1$-glucose as the carbon source. NMR samples contained 1.0−1.2 mM SlyD in 20 mM HEPES pH 7.5. All samples contained 10% (v/v) D_2O.

NMR Spectroscopy. ^{13}C L-TROSY-CPMG relaxation dispersion experiments[27] were performed at natural abundance on an 8 mM BPTI sample at 35 and 65 °C and a static magnetic field strength of B_0 = 11.7 T. Twelve experiments were conducted with refocusing frequencies of ν_{CP} = 33, 67, 100, 167, 167, 233, 333, 433, 533, 667, 833, and 1000 Hz at 35 °C and ν_{CP} = 50, 100, 200, 300, 300, 400, 500, 600, 700, 800, 900, and 1000 Hz at 65 °C. The relaxation period in the relaxation dispersion experiments was adjusted so that $I(T) \approx 0.5I(0)$ or higher, where $I(0)$ is the intensity at T = 0. In addition, ^{1}H−^{13}C TROSY spectra were acquired at B_0 = 11.7 T and 5 °C. ^{13}C L-TROSY-CPMG relaxation dispersion experiments were performed on SlyD labeled with 1-$^{13}C_1$-glucose or 2-$^{13}C_1$-glucose at 25 °C and 11.7 T and ν_{CP}= 50, 100, 100, 150, 200, 200, 300, 400, 400, 500, 600, 700, 800, 900, and 1000 Hz. ^{1}H−^{13}C heteronuclear single-quantum coherence (HSQC) spectra were recorded with ^{13}C CPMG decoupling applied during the acquisition period, using refocusing frequencies nearly identical to those employed in the ^{13}C L-TROSY-CPMG experiment of BPTI at 35 °C and in the density matrix calculations: ν_{CP}= 0, 33, 67, 100, 134, 167, 202, 235, 271, 302, 334, 439, and 554 Hz. These experiments were performed on the 1-$^{13}C_1$-glucose-labeled sample of SlyD at 25 °C and 11.7 T.

Density Matrix Calculations. The evolution of the spin density operator in Liouville space during the ^{13}C L-TROSY-CPMG experiment was simulated by way of the homogeneous master equation[31−33] as implemented in QSim.[34] The simulations covered the full CPMG relaxation period, including the central S^3CT element.[27,35] Initial simulations treated a four-spin system to investigate the influence of strong $^2J_{CC}$ or $^4J_{HH}$ couplings (both assumed to be ≤2 Hz) on the relaxation dispersions. The final simulations were performed on a three-spin system comprising the directly coupled $^{13}C^{\delta_1}$−$^1H^{\delta_1}$ spin pair of interest ($^1J_{CH}$ = 155 Hz) and the $^1H^{\varepsilon_1}$ spin, which is scalar-coupled to $^1H^{\delta_1}$ ($^3J_{HH}$ = 8 Hz), with or without symmetric exchange between the two sides of the ring (p_A = p_B = 0.5). The frequency difference between $^1H^{\delta_1}$ and $^1H^{\varepsilon_1}$ ($\Delta\omega_1$) was varied and that between $^1H^{\delta_2}$ and $^1H^{\varepsilon_2}$ was set to $\Delta\omega_2/2\pi$ = 200 Hz; in practice, any value of $\Delta\omega_2/2\pi$ > 60 Hz leads to a weakly coupled ^{1}H spectrum in the limit of fast ring flips. In addition, the exchange rate ($k_{ex} = 2k_{flip}$) was varied. For simplicity and maximal effect, $\Delta\omega$ between $^{13}C^{\delta_1}$ and $^{13}C^{\delta_2}$ was set to 0. Control simulations with a finite ^{13}C chemical shift difference show the same effect on the dispersion profile due to strong coupling between protons as in the absence of a ^{13}C chemical shift difference. The decay of the magnetization selected for in the TROSY-CPMG experiment was calculated to yield the apparent relaxation rate, R_{app}, as a function of ν_{CP}, $\Delta\omega_1$, and k_{ex}.

RESULTS AND DISCUSSION

We measured natural abundance ^{13}C L-TROSY-CPMG relaxation rates in BPTI as a function of the CPMG refocusing frequency. The resulting CPMG relaxation dispersion curves obtained for $^{13}C^{\delta}$ and $^{13}C^{\varepsilon}$ spins of Y21 at 35 °C reveal an anomalous profile, resembling relaxation dispersion curves that have been turned upside down (Figure 1A). For reference, we also include data for the protein SlyD.[30] Figure 1B shows a

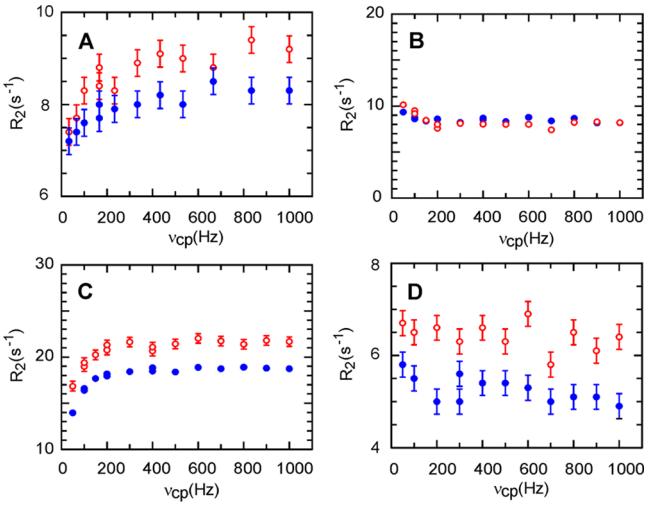

Figure 1. ^{13}C L-TROSY-CPMG relaxation dispersion profiles. The data for BPTI Y21 were acquired at 308 K (A) and 338 K (D) and those for SlyD Y92 (B) and F79 (C) were acquired at 298 K. Solid blue and open red points represent the δ* and ε* sites, respectively. The samples contained (A, D) 8 mM BPTI at natural abundance in water pH 7.1, and (B, C) 1.0−1.2 mM SlyD, specifically labeled using 1-$^{13}C_1$-glucose or 2-$^{13}C_1$-glucose, in 20 mM HEPES pH 7.5.

dx.doi.org/10.1021/jp4058065 | J. Phys. Chem. B 2013, 117, 9241−9247

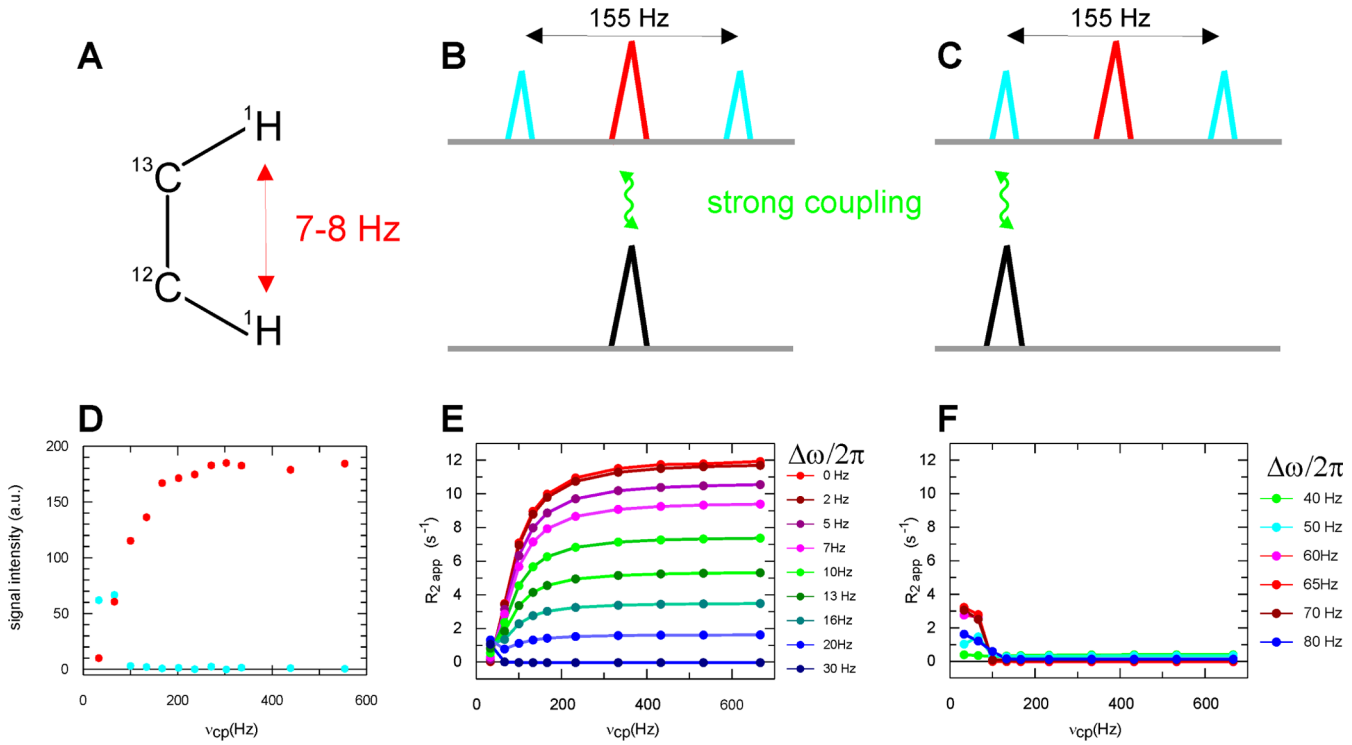

Figure 2. ^{13}C TROSY-CPMG relaxation dispersions caused by strong ^{1}H−^{1}H coupling in aromatic spin systems. (A) Schematic outline of the spin system. The ^{1}H covalently bound to the ^{13}C of interest is scalar-coupled ($^{3}J_{HH}$ = 7−8 Hz) to its vicinal ^{1}H neighbor, which is attached to ^{12}C. Two basic scenarios of frequency matching in the ^{1}H spectrum are encountered for the present spin system: the singlet of the ^{12}C-bound proton (black) matches either the (B) collapsed (^{13}C-decoupled) doublet of the ^{13}C-bound proton (red), $\tan(2\theta_B) = 2\pi^3 J_{HH}/\Delta\omega$; or (C) one of the two lines of the non-decoupled doublet of the ^{13}C-bound proton (cyan), $\tan(2\theta_C) = 2\pi^3 J_{HH}/(\Delta\omega \pm {}^{1}J_{CH})$. Panel C illustrates matching only with the left-hand line of the doublet; the corresponding case for the right-hand line yields identical results. In panels B and C, the splitting due to the $^{3}J_{HH}$ coupling has been omitted for clarity. (D) The signal intensities of the central (red) and dominant outer (cyan) lines are shown as a function of ^{13}C CPMG refocusing frequency, as determined experimentally for Y92 δ* in SlyD. (E) ^{13}C CPMG relaxation dispersions calculated for scenario B and a range of frequency differences between the two protons (colored lines). $^{3}J_{HH}$ = 8 Hz in the calculations. (F) Content is as in panel E but is for scenario C. $\Delta\omega/2\pi$ refers to the frequency difference between the central lines. The evolution of the spin density operator in Liouville space during the ^{13}C L-TROSY-CPMG experiment was simulated using QSim.[34]

typical dispersion profile for residue Y92 in SlyD, while the data measured for F79 in SlyD (Figure 1C) are similar to those for Y21 in BPTI. Below we demonstrate that the anomalous dispersion profiles can be interpreted in favorable cases to yield unique information on the flip rates of aromatic rings showing single-peak NMR spectra.

^{13}C CPMG Relaxation Dispersions Are Affected by Strong ^{3}J ^{1}H−^{1}H Couplings. The anomalous dispersion profiles (Figure 1A,C) arise because the relaxation of the TROSY spin state is affected by strong scalar coupling between the ^{13}C-attached proton and its vicinal proton neighbor. In essence, spin-state selection becomes corrupted because strong coupling mixes the $|\alpha\beta\rangle$ and $|\beta\alpha\rangle$ ^{1}H spin states that are eigenfunctions of the Hamiltonian in the weak coupling limit, and consequently the TROSY magnetization component decays because of coherent evolution into magnetizations that are not refocused during the CPMG relaxation delay. Similar considerations apply to the evolution of the antiphase term in regular (non-TROSY) CPMG experiments. The basic theory of strong coupling involving passive spins in CPMG experiments has been outlined,[36] and the specific case of strong residual dipolar couplings between backbone amide protons in aligned media and their effect on ^{15}N TROSY-CPMG experiments has been described previously.[37] The present case involves a three-spin system comprising the two coupled protons, only one of which is covalently attached to a ^{13}C nucleus (Figure 2A). Thus, there are two basic scenarios of strong scalar coupling, depending on which resonance lines overlap in the ^{1}H spectrum, as outlined in Figure 2B,C and referred to in the following as scenario B and scenario C, respectively. The strong coupling parameter θ, defined by the relationship $\tan(2\theta) = 2\pi J/\Delta\omega$, describes the extent of mixing of the $|\alpha\beta\rangle$ and $|\beta\alpha\rangle$ eigenfunctions (derived for the case of weak coupling) to yield the generalized eigenfunctions $|\alpha\beta\rangle \cos\theta + |\beta\alpha\rangle \sin\theta$ and $|\alpha\beta\rangle \sin\theta - |\beta\alpha\rangle \cos\theta$.[38] The two basic strong coupling scenarios encountered here correspond to $\tan(2\theta_B) = 2\pi^3 J_{HH}/\Delta\omega$ and $\tan(2\theta_C) = 2\pi^3 J_{HH}/(\Delta\omega \pm {}^{1}J_{CH})$. On the basis of these two scenarios, we analyzed the anomalous dispersion profiles in more detail, as described below.

To extract information on aromatic ring-flip rates from the anomalous CPMG dispersion profiles, we systematically investigated the effects of the pertinent parameters on the apparent ^{13}C relaxation rates. We examined the effects of various scalar couplings on the ^{13}C L-TROSY-CPMG experiment by numerical simulation of the evolution of the density matrix during the CPMG period. First, we tested the influence of strong coupling due to the various possible scalar coupling constants present in an aromatic ring; these simulations included $^{2}J_{CC}$ and $^{4}J_{HH}$ couplings, which were both assumed to be <2 Hz,[39−41] as well as $^{3}J_{HH}$ couplings of 7−8 Hz.[41] The results show that the $^{2}J_{CC}$ and $^{4}J_{HH}$ couplings do not have any significant impact on the evolution of the density operator and

dx.doi.org/10.1021/jp4058065 | J. Phys. Chem. B 2013, 117, 9241−9247

can be safely neglected, irrespective of the chemical shift difference between the coupled spins. By contrast, $^3J_{HH}$ has a strong effect and leads to a significant decay of the TROSY magnetization, as also observed experimentally (Figure 1). Thus, it is sufficient to include in the analysis a minimal three-spin system comprising the two vicinal protons and the monitored ^{13}C nucleus, which is covalently attached to one of the protons (Figure 2A). We analyzed how the apparent relaxation rate depends on the degree of strong coupling, taking $^1J_{HC}$ = 155 Hz and $^3J_{HH}$ = 8 Hz as fixed parameters while varying the chemical shift difference between the two vicinal protons, $\Delta\omega$. The dependence of the apparent relaxation rate on the CPMG refocusing frequency can be appreciated by considering the effect of the ^{13}C CPMG pulse train on the ^{1}H spectrum. In scenario B (Figure 2B), the strong coupling regime is reached gradually as the central line of the ^{1}H spectrum grows in intensity with increasingly higher values of ν_{CP} (Figure 2E). Conversely, in scenario C (Figure 2C) the two ^{1}H spins are strongly coupled prior to complete ^{13}C decoupling, such that the ^{1}H spectrum moves away from the strong coupling regime as ν_{CP} approaches infinity (Figure 2F). The two scenarios result in relaxation dispersion profiles that are not mirror images of one another because the central and outer lines of the ^{1}H spectrum are not affected in the same way by the decoupling ^{13}C CPMG sequence. CPMG decoupling gives rise to sidebands in the ^{1}H spectrum that are offset from the central (decoupled) line by $n\nu_{CP}$, where n is an integer.[42] In scenario C, the strong coupling parameter θ will therefore depend on both ν_{CP} and the frequency difference between the central lines of the two protons. Hence, the maximum relaxation rate might occur at an intermediate value of ν_{CP} if this leads to a frequency match between the ^{12}C-attached proton and a sideband of the ^{13}C-attached proton, e.g., $\Delta\omega = \omega_\varepsilon - (\omega_\delta \pm n2\pi\nu_{CP})$. We verified this by measuring the intensities of the central (decoupled) and outer (non-decoupled or sideband) ^{1}H peaks in ^{1}H−^{13}C HSQC spectra acquired with ^{13}C decoupling brought about using a CPMG train that was the same as that employed in the dispersion experiments (see Supporting Information, Figure S1). Figure 2D shows a representative example of these data demonstrating that the resulting peak intensities indeed follow a dependence on the CPMG frequency that is the same as that observed in the experimental and simulated dispersion profiles (Figures 1A,C and 2E,F). We conclude that the effect of strong ^{1}H−^{1}H coupling in the ^{13}C L-TROSY-CPMG experiment depends on ν_{CP} in a way that is described by the relative ^{1}H resonance frequencies and the decoupling efficiency and sideband patterns of the ^{13}C CPMG pulse train.

The simulated relaxation dispersion profiles for scenario B (Figure 2E) clearly demonstrate that strong $^3J_{HH}$ coupling has a dramatic influence on the apparent relaxation rate and gives rise to behavior that is the same as that observed experimentally (Figure 1). As expected, the effect on the dispersions is maximal for a perfect proton frequency match ($\Delta\omega$ = 0) and is observable for values of about $\Delta\omega/2\pi$ < 20 Hz = 2.5 $^3J_{HH}$. Scenario C, on the other hand, results in a much weaker effect that is visible only at low values of the ^{13}C CPMG refocusing frequency, ν_{CP} (Figure 2F). For this reason, dispersions originating from scenario C would be difficult to characterize experimentally, whereas scenario B results in dispersion profiles that can be interpreted quantitatively.

Ring-Flips Attenuate Anomalous Relaxation Dispersions Caused by Strong ^{1}H−^{1}H Couplings. The results presented in Figure 2E,F represent the static case where strong $^3J_{HH}$ coupling prevails. We next addressed the effect of symmetric exchange of the three-spin system between two sites characterized by strong and weak coupling, with $\Delta\omega_1/2\pi$ = 0 Hz and $\Delta\omega_2/2\pi$ = 200 Hz, where $\Delta\omega_1$ and $\Delta\omega_2$ denote the chemical shift difference between the δ and ε protons on either side of the ring. Figure 3 shows that the effect of such one-sided

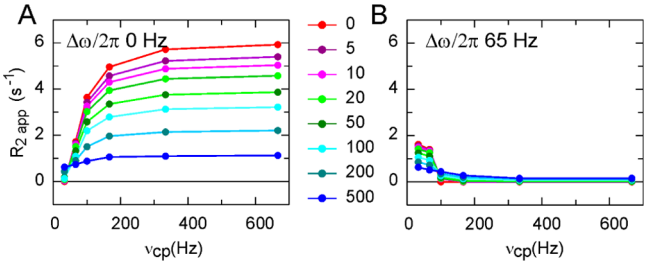

Figure 3. The effect of symmetric exchange between two sites with weak and strong ^{1}H−^{1}H couplings on the CPMG relaxation dispersions. Dispersions arising from (A) scenario B with $\Delta\omega_1/2\pi$ = 0 Hz and (B) scenario C with $\Delta\omega_1/2\pi$ = 65 Hz. In panels A and B, $\Delta\omega_2/2\pi$ = 200 Hz and $^3J_{HH}$ = 8 Hz. The colored lines indicate different values of k_{ex} in units of inverse seconds.

strong coupling is markedly dependent on the exchange rate, $k_{ex} = 2k_{flip}$. As the exchange rate increases, the effect of strong coupling becomes reduced by motional averaging. Importantly, significant dispersion, such as that presented in Figure 1, is observed only for relatively slow flip rates, k_{flip} < 250 s^{-1}.

Figure 3 represents a limiting case where exchange has the maximum effect on the relaxation dispersion curve. In general, the extent of exchange-mediated decoupling depends on the degree of strong coupling on the two sides of the ring: if the coupling is equally strong on both sides of the ring, then exchange does not reduce the apparent relaxation rate and the dispersion curve does not contain any information on the ring-flip dynamics; if one side is strongly coupled and the other is not fully in the weak coupling regime, then the apparent relaxation rate is reduced by exchange less than in the case described by Figure 3. To determine k_{flip} from anomalous CPMG dispersions it is therefore necessary to evaluate the degree of strong coupling in the specific spin system, which amounts to determining $\Delta\omega_1$ and $\Delta\omega_2$; $^3J_{HH}$ is expected to be essentially invariant in aromatic rings. It is impossible to determine $\Delta\omega_1$ and $\Delta\omega_2$ directly from the spectrum if only a single peak is observed for each pair of δ and ε protons, as is the case for Y21 in BPTI. However, the sum of $\Delta\omega_1$ and $\Delta\omega_2$ is bounded by the shift difference between the observed δ and ε peaks as $\Delta\omega_{obs} = 0.5(\Delta\omega_1 + \Delta\omega_2)$, and it is thus possible to identify cases where the coupling is strong on both sides of the ring, or only on one side.

Slow Ring Flips Detected for Y21 in BPTI. The anomalous dispersion profiles shown in Figure 1A,C directly imply that strong coupling applies on (at least) one side of the ring, which in turn implies that $\Delta\omega_1/2\pi$ < 20 Hz (Figure 2E). Hence, if $\Delta\omega_{obs}/2\pi$ > 20 Hz, then it can be concluded that the δ and ε protons are strongly coupled on only one side of the ring. This scenario applies to Y21 in BPTI, for which $\Delta\omega_{obs}/2\pi$ = 42 ± 2 Hz at 11.7 T (Figure 4). By contrast, F79 in SlyD has $\Delta\omega_{obs}/2\pi$ = 2 ± 2 Hz and is thus strongly coupled on both sides of the ring; in fact, SlyD does not have any aromatic spin

dx.doi.org/10.1021/jp4058065 | J. Phys. Chem. B 2013, 117, 9241−9247

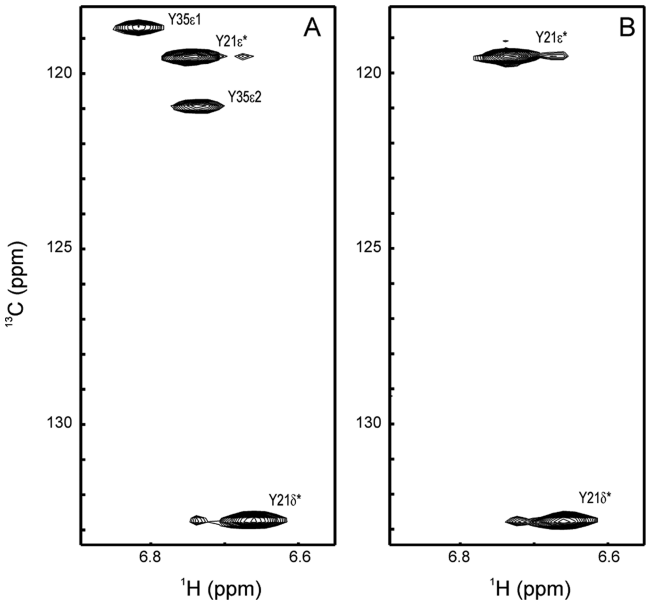

Figure 4. Aromatic region covering the δ* and ε* cross-peaks of Y21 in ^{1}H−^{13}C TROSY spectra recorded on a 8 mM sample of BPTI in water pH 7.1 at a static magnetic field strength of 11.7 T and temperatures of 35 °C (A) and 65 °C (B). The spectral region also includes the cross-peaks of ε1 and ε2 of Y35, which are broadened beyond detection at 65 °C.

systems that are strongly coupled on only one side of the ring. Taken together, the dispersion data and $\Delta\omega_{obs}$ thus establish that the Y21 aromatic ring flips with a rate $k_{flip} < 100$ s^{-1}. This result differs markedly from previous estimates of $k_{flip} > 10^4$–10^6 s^{-1}, which were based on measured linewidths and assumptions regarding the chemical shift differences between the exchanging sites[8,29,43] rather than on direct rate measurements. Given the slow flip rate measured here for Y21, we conclude that the chemical shifts of the δ and ε positions of both ^{1}H and ^{13}C are nearly degenerate.

As is evident from Figure 3, anomalous relaxation dispersions show a strong dependence on the flip rate and should therefore also exhibit a significant temperature dependence. To address this point, we acquired ^{13}C L-TROSY-CPMG dispersions for BPTI at higher temperatures. We observe that the anomalous dispersion disappears at 65 °C (Figure 1D), indicating that at this temperature $k_{flip} > 250$ s^{-1} (Figure 3). Assuming simple Arrhenius behavior we thus expect a flip rate of 30 s$^{-1} < k_{flip} <$ 100 s^{-1} at 35 °C for Y21, which is on par with the rates determined previously for residues Y23, Y35, and F45 in BPTI.[8,29] The latter three residues give rise to separate peaks for the δ1/δ2 and ε1/ε2 positions at low or ambient temperatures, and their flip rates are consequently well-determined. Figure 5 shows that Y21 is located near Y23 and F45, suggesting that this entire region is perhaps less flexible and that the breathing motions that make ring flips possible are less local in character than previously recognized.

Notably, a recent 1 ms MD simulation of BPTI also placed Y21 in the category of more slowly flipping rings together with Y23, Y35, and F45.[12] Similarly, a 1.27 μs MD trajectory at high temperature (375 K) did not result in any ring flips of Y21.[43] The previous assignment of Y21 to the group of the most rapidly flipping aromatic rings in BPTI[8] is inconsistent with the MD results. Our result thus resolves this issue by validating the MD trajectories in qualitative terms. However, the flip rates

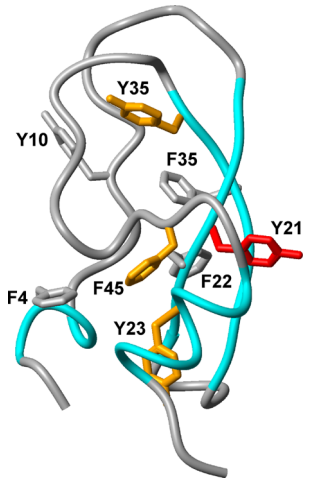

Figure 5. Location of aromatic side chains in the structure of BPTI. The backbone is shown in tube representation with secondary structure elements highlighted in cyan, and Phe and Tyr side chains are shown in stick representation. Slowly flipping rings are highlighted in color: red, Y21 (this work); gold, Y23, Y35 and F45.[8,10] Aromatic rings that have been inferred to flip rapidly are colored gray.[8,10] The figure was made using PDB coordinates 5PTI[45] and MolMol.[46].

estimated from the 1 ms MD trajectory for the group of slowly flipping aromatics are 1–2 orders of magnitude greater than those obtained by experiment. This quantitative discrepancy suggests that continued refinement of force fields and molecular simulation methodology is necessary to capture the complex dynamics associated with the deceptively simple process of a ring flip. As longer time scale MD trajectories become increasingly accessible, it is critical that accurate experimental data are available for validation purposes. Aromatic ring flips arguably represent a valuable and challenging benchmark because they do not appear to depend in any simple manner on the potential function of the local torsion angles but rather on a larger set of degrees of freedom, including the surrounding protein matrix. Furthermore, ring flips presumably reflect dynamics on a wide range of time scales, which is attractive for the purpose of validation. We therefore believe that novel experimental methods providing improved estimates of aromatic ring-flip rates will continue to serve an important role in the field of protein dynamics.

■ CONCLUSIONS

We have demonstrated that anomalous CPMG relaxation dispersion profiles acquired on aromatic ^{13}C spins can be interpreted to yield unique information on ring-flip rates. Using this technique, we have identified for the first time slow ring flips of an aromatic residue exhibiting a single-peak NMR spectrum for the two exchanging spins. Our result contrasts with the common interpretation, exemplified by the statement in classic publications that "symmetric" spectra (i.e., where a single peak is observed for the two nuclei) observed for aromatic rings in globular proteins can be taken as conclusive evidence for rapid ring rotation.[8,44] It is worth noting that until now slow ring flips have been possible to detect only for cases where separate peaks are observed for the two nuclei, which obviously limits the strength of the inferences made previously. At present, it is an open question whether our results might be a first indication that slow ring flips are more common than previously believed, or whether Y21 in BPTI is an extraordinary

dx.doi.org/10.1021/jp4058065 | J. Phys. Chem. B 2013, 117, 9241−9247

case with its virtually degenerate ^{1}H and ^{13}C resonances. This question can be addressed only by future investigations of other proteins.

■ ASSOCIATED CONTENT

Supporting Information

Figure showing the effect of ^{13}C decoupling on the ^{1}H spectrum. This material is available free of charge via the Internet at http://pubs.acs.org.

■ AUTHOR INFORMATION

Corresponding Author

*E-mail: mikael.akke@bpc.lu.se.

Notes

The authors declare no competing financial interest.

■ ACKNOWLEDGMENTS

We thank Bertil Halle for the BPTI sample. This research was supported by the Swedish Research Council (621-2010-4912; 822-2005-2915), the Göran Gustafsson Foundation for Research in Natural Sciences and Medicine, and the Knut and Alice Wallenberg Foundation. U.W. was supported by an EMBO long-term fellowship. M.R. was supported by a postdoctoral fellowship funded by the Swedish Research Council (623-2009-800).

■ ABBREVIATIONS

BPTI, bovine pancreatic trypsin inhibitor; CPMG, Carr−Purcell−Meiboom−Gill; HSQC, heteronuclear single-quantum coherence; L-TROSY, longitudinal and transverse relaxation-optimized spectroscopy; TROSY, transverse relaxation-optimized spectroscopy; SlyD, sensitive to lysis D protein from *Thermus thermophilus*

■ REFERENCES

(1) Burley, S. K.; Petsko, G. A. Aromatic-Aromatic Interaction−A Mechanism of Protein-Structure Stabilization. *Science* **1985**, *229*, 23−28.

(2) Campbell, I. D.; Dobson, C. M.; Williams, R. J. P. Proton Magnetic-Resonance Studies of Tyrosine Residues of Hen Lysozyme-Assignment and Detection of Conformational Mobility. *Proc. R. Soc. B* **1975**, *189*, 503−509.

(3) Hull, W. E.; Sykes, B. D. Fluorotyrosine Alkaline Phosphatase. Internal Mobility of Individual Tyrosines and the Role of Chemical Shift Anisotropy as a Fluorine-19 Nuclear Spin Relaxation Mechanism in Proteins. *J. Mol. Biol.* **1975**, *98*, 121−153.

(4) Wüthrich, K.; Wagner, G. NMR Investigations of the Dynamics of the Aromatic Amino Acid Residues in the Basic Pancreatic Trypsin Inhibitor. *FEBS Lett.* **1975**, *50*, 265−268.

(5) Wagner, G. Activation Volumes for the Rotational Motion of Interior Aromatic Rings in Globular-Proteins Determined by High-Resolution ^{1}H NMR at Variable Pressure. *FEBS Lett.* **1980**, *112*, 280−284.

(6) Hattori, M.; Li, H.; Yamada, H.; Akasaka, K.; Hengstenberg, W.; Gronwald, W.; Kalbitzer, H. R. Infrequent Cavity-Forming Fluctuations in HPr from *Staphylococcus carnosus* Revealed by Pressure- and Temperature-Dependent Tyrosine Ring Flips. *Protein Sci.* **2004**, *13*, 3104−3114.

(7) Li, H.; Yamada, H.; Akasaka, K. Effect of Pressure on the Tertiary Structure and Dynamics of Folded Basic Pancreatic Trypsin Inhibitor. *Biophys. J.* **1999**, *77*, 2801−2812.

(8) Wagner, G.; Demarco, A.; Wüthrich, K. Dynamics of Aromatic Amino-Acid Residues in Globular Conformation of Basic Pancreatic Trypsin-Inhibitor (BPTI) I. ^{1}H NMR-Studies. *Biophys. Struct. Mech.* **1976**, *2*, 139−158.

(9) Rao, D. K.; Bhuyan, A. K. Complexity of Aromatic Ring-Flip Motions in Proteins: Y97 Ring Dynamics in Cytochrome C Observed by Cross-Relaxation Suppressed Exchange NMR Spectroscopy. *J. Biomol. NMR* **2007**, *39*, 187−196.

(10) Wagner, G.; Brühwiler, D.; Wüthrich, K. Reinvestigation of the Aromatic Side-Chains in the Basic Pancreatic Trypsin-Inhibitor by Heteronuclear Two-Dimensional Nuclear-Magnetic-Resonance. *J. Mol. Biol.* **1987**, *196*, 227−231.

(11) Wong, K. B.; Daggett, V. Barstar Has a Highly Dynamic Hydrophobic Core: Evidence from Molecular Dynamics Simulations and Nuclear Magnetic Resonance Relaxation Data. *Biochemistry* **1998**, *37*, 11182−11192.

(12) Shaw, D. E.; Maragakis, P.; Lindorff-Larsen, K.; Piana, S.; Dror, R. O.; Eastwood, M. P.; Bank, J. A.; Jumper, J. M.; Salmon, J. K.; Shan, Y. B.; et al. Atomic-Level Characterization of the Structural Dynamics of Proteins. *Science* **2010**, *330*, 341−346.

(13) Palmer, A. G.; Kroenke, C. D.; Loria, J. P. Nuclear Magnetic Resonance Methods for Quantifying Microsecond-to-Millisecond Motions in Biological Macromolecules. *Methods Enzymol.* **2001**, *339*, 204−238.

(14) Akke, M. NMR Methods for Characterizing Microsecond-Millisecond Dynamics in Recognition and Catalysis. *Curr. Opin. Struct. Biol.* **2002**, *12*, 642−647.

(15) Gutowsky, H. S.; Saika, A. Dissociation, Chemical Exchange, and the Proton Magnetic Resonance in Some Aqueous Electrolytes. *J. Chem. Phys.* **1953**, *21*, 1688−1694.

(16) Igumenova, T. I.; Brath, U.; Akke, M.; Palmer, A. G. Characterization of Chemical Exchange Using Residual Dipolar Coupling. *J. Am. Chem. Soc.* **2007**, *129*, 13396−13397.

(17) Vallurupalli, P.; Hansen, D. F.; Stollar, E.; Meirovitch, E.; Kay, L. E. Measurement of Bond Vector Orientations in Invisible Excited States of Proteins. *Proc. Natl. Acad. Sci. U.S.A.* **2007**, *104*, 18473−18477.

(18) Carr, H. Y.; Purcell, E. M. Effects of Diffusion on Free Precession in Nuclear Magnetic Resonance Experiments. *Phys. Rev.* **1954**, *94*, 630−638.

(19) Meiboom, S.; Gill, D. Modified Spin-Echo Method for Measuring Nuclear Spin Relaxation Times. *Rev. Sci. Instrum.* **1958**, *29*, 688−691.

(20) Eisenmesser, E. Z.; Bosco, D. A.; Akke, M.; Kern, D. Enzyme Dynamics During Catalysis. *Science* **2002**, *295*, 1520−1523.

(21) Grey, M. J.; Wang, C.; Palmer, A. G. Disulfide Bond Isomerization in Basic Pancreatic Trypsin Inhibitor: Multisite Chemical Exchange Quantified by CPMG Relaxation Dispersion and Chemical Shift Modeling. *J. Am. Chem. Soc.* **2003**, *125*, 14324−14335.

(22) Sprangers, R.; Gribun, A.; Hwang, P. M.; Houry, W. A.; Kay, L. E. Quantitative NMR Spectroscopy of Supramolecular Complexes: Dynamic Side Pores in ClpP Are Important for Product Release. *Proc. Natl. Acad. Sci. U.S.A.* **2005**, *102*, 16678−16683.

(23) Boehr, D. D.; McElheny, D.; Dyson, H. J.; Wright, P. E. The Dynamic Energy Landscape of Dihydrofolate Reductase Catalysis. *Science* **2006**, *313*, 1638−1642.

(24) Brüschweiler, S.; Schanda, P.; Kloiber, K.; Brutscher, B.; Kontaxis, G.; Konrat, R.; Tollinger, M. Direct Observation of the Dynamic Process Underlying Allosteric Signal Transmission. *J. Am. Chem. Soc.* **2009**, *131*, 3063−3068.

(25) Lipchock, J. M.; Loria, J. P. Nanometer Propagation of Millisecond Motions in V-Type Allostery. *Structure* **2010**, *18*, 1596−1607.

(26) Weininger, U.; Diehl, C.; Akke, M. ^{13}C Relaxation Experiments for Aromatic Side Chains Employing Longitudinal- and Transverse-Relaxation Optimized NMR Spectroscopy. *J. Biomol. NMR* **2012**, *53*, 181−190.

(27) Weininger, U.; Respondek, M.; Akke, M. Conformational Exchange of Aromatic Side Chains Characterized by L-Optimized TROSY-Selected ^{13}C CPMG Relaxation Dispersion. *J. Biomol. NMR* **2012**, *54*, 9−14.

(28) Ulrich, E. L.; Akutsu, H.; Doreleijers, J. F.; Harano, Y.; Ioannidis, Y. E.; Lin, J.; Livny, M.; Mading, S.; Maziuk, D.; Miller, Z.; et al. BioMagResBank. *Nucleic Acids Res.* **2008**, *36*, D402−D408.
(29) Skalicky, J. J.; Mills, J. L.; Sharma, S.; Szyperski, T. Aromatic Ring-Flipping in Supercooled Water: Implications for NMR-Based Structural Biology of Proteins. *J. Am. Chem. Soc.* **2001**, *123*, 388−397.
(30) Löw, C.; Neumann, P.; Tidow, H.; Weininger, U.; Haupt, C.; Friedrich-Epler, B.; Scholz, C.; Stubbs, M. T.; Balbach, J. Crystal Structure Determination and Functional Characterization of the Metallochaperone SlyD from *Thermus thermophilus*. *J. Mol. Biol.* **2010**, *398*, 375−390.
(31) Jeener, J. Superoperators in Magnetic Resonance. *Adv. Magn. Reson.* **1982**, *10*, 1−51.
(32) Levitt, M. H.; Dibari, L. Steady-State in Magnetic-Resonance Pulse Experiments. *Phys. Rev. Lett.* **1992**, *69*, 3124−3127.
(33) Levitt, M. H.; Di Bari, L. The Homogeneous Master Equation and the Manipulation of Relaxation Networks. *Bull. Magn. Reson.* **1994**, *16*, 94−114.
(34) Helgstrand, M.; Allard, P. QSim, A Program for NMR Simulations. *J. Biomol. NMR* **2004**, *30*, 71−80.
(35) Sørensen, M. D.; Meissner, A.; Sørensen, O. W. Spin-State-Selective Coherence Transfer via Intermediate States of Two-Spin Coherence in IS Spin Systems: Application to E.COSY-Type Measurement of J Coupling Constants. *J. Biomol. NMR* **1997**, *10*, 181−186.
(36) Kumar, A.; Ernst, R. R. Influence of Nonresonant Nuclei on NMR Spin Echoes in Liquids and in Solids. *J. Magn. Reson.* **1976**, *24*, 425−447.
(37) van Ingen, H.; Korzhnev, D. M.; Kay, L. E. An Analysis of the Effects of $^{1}H^{N}-^{1}H^{N}$ Dipolar Couplings on the Measurement of Amide Bond Vector Orientations in Invisible Protein States by Relaxation Dispersion NMR. *J. Phys. Chem. B* **2009**, *113*, 9968−9977.
(38) Cavanagh, J.; Fairbrother, W. J.; Palmer, A. G.; Rance, M.; Skelton, N. J. *Protein NMR Spectroscopy: Principles and Practice*, 2nd ed.; Elsevier Academic Press: San Diego, CA, 2007.
(39) Kaski, J.; Vaara, J.; Jokisaari, J. $^{13}C-^{13}C$ Spin−Spin Coupling Tensors in Benzene as Determined Experimentally by Liquid Crystal NMR and Theoretically by *ab Initio* Calculations. *J. Am. Chem. Soc.* **1996**, *118*, 8879−8886.
(40) Witanowski, M.; Kamienska-Trela, K.; Biedrzycka, Z. Indirect Carbon-Carbon Couplings across One, Two and Three Bonds in Substituted Benzenes: Experiment and Theory. *J. Mol. Struct.* **2007**, *844*, 13−20.
(41) Laatikainen, R.; Ratilainen, J.; Sebastian, R.; Santa, H. NMR Study of Aromatic−Aromatic Interactions for Benzene and Some Other Fundamental Aromatic Systems Using Alignment of Aromatics in Strong Magnetic Field. *J. Am. Chem. Soc.* **1995**, *117*, 11006−11010.
(42) Shaka, A. J.; Keeler, J. Broadband Spin Decoupling in Isotropic Liquids. *Prog. Nucl. Magn. Reson. Spectrosc.* **1987**, *19*, 47−129.
(43) Sathyamoorthy, B.; Singarapu, K. K.; Garcia, A. E.; Szyperski, T. Protein Conformational Space Populated in Solution Probed with Aromatic Residual Dipolar $^{13}C-^{1}H$ Couplings. *ChemBioChem* **2013**, *14*, 685−688.
(44) Wüthrich, K.; Wagner, G. Internal Motion in Globular Proteins. *Trends Biochem. Sci.* **1978**, *3*, 227−230.
(45) Wlodawer, A.; Walter, J.; Huber, R.; Sjolin, L. Structure of Bovine Pancreatic Trypsin Inhibitor: Results of Joint Neutron and X-Ray Refinement of Crystal Form II. *J. Mol. Biol.* **1984**, *180*, 301−329.
(46) Koradi, R.; Billeter, M.; Wüthrich, K. MOLMOL: A Program for Display and Analysis of Macromolecular Structures. *J. Mol. Graphics* **1996**, *14*, 51−55.